14th International Symposium on Turbulence and Shear Flow Phenomena (TSFP14)
Heidelberg, Germany, July 28–31, 2026

ALTERING NEAR-WALL TURBULENCE VIA HELMHOLTZ RESONATORS WITH INCLINED ORIFICES IN WALL-BOUNDED FLOWS

Abdelrahman H.A.S. Hassanein
Faculty of Aerospace Engineering
Delft University of Technology
2629 HS Delft, The Netherlands
a.h.hassanein@tudelft.nl

Davide Modesti
Gran Sasso Science Institute
Viale Francesco Crispi 7
67100 L'Aquila, Italy

Woutijn J. Baars
Faculty of Aerospace Engineering
Delft University of Technology
2629 HS Delft, The Netherlands

ABSTRACT

We explore the use of orifice inclination of a miniature Helmholtz resonator as a means of affecting the control authority. It is hypothesised that inclining the orifice shifts the phase between the induced velocity fluctuations of the resonator and the wall-pressure fluctuations exciting it, thereby altering the interaction with the turbulence. Time-resolved planar particle image velocimetry is employed for flow measurements across five inclination angles ranging from $\theta = -70^\circ$ to $\theta = 70^\circ$. The results show that the most negatively inclined case amplifies velocity fluctuations over a broader range of frequencies compared to the non-inclined orifice, while the most positively inclined case attenuates velocity fluctuations over a broader range and amplifies a narrower band. This frequency-selective behaviour is attributed to a shift in the phase between the induced wall-normal velocity and the wall-pressure fluctuations exciting the resonator. Examination of the phase between the cavity pressure and the wall-normal velocity fluctuations above the orifice confirms that inclination can induce a predetermined shift in the phase. This skewing is found to be governed by the ratio of the apparent orifice diameter to the wavelength of the velocity fluctuations. These findings highlight the great potential of using Helmholtz resonators for controlling the near-wall turbulence.

INTRODUCTION

Helmholtz resonators (HRs) are passive devices characterised by a frequency-dependent velocity response to pressure excitations. They thereby hold promise in the realm of surface modification as a means to control wall-bounded turbulence (Flynn *et al.*, 1990; Dacome *et al.*, 2024; Hassanein *et al.*, 2024). Despite this immense potential, recent work (Dacome *et al.*, 2024; Hassanein *et al.*, 2024) shows that the response realized by a conventional miniature Helmholtz resonator has an inherent duality: it amplifies velocity fluctuations at frequencies equal to or higher than resonance, while attenuating velocity fluctuations at lower frequencies. In this work, we explore a simple geometric modification with the aim of skewing this duality. We therefore pose the following question: **can inclining the orifice of a miniature Helmholtz resonator break its inherent response duality, biasing toward broadband amplification or broadband attenuation of velocity fluctuations?**

Earlier work in the literature looked at the influence of HRs on wall-bounded turbulence when the resonator's orifice dimensions are in the order of $d \sim \delta$. Flynn *et al.* (1990) demonstrated that the natural frequency of a macro-scale HR can be tuned to interact with near-wall turbulence, leading to increased streamwise and wall-normal velocity fluctuations downstream. More recently, Dacome *et al.* (2024) studied miniature HRs (with $d \sim \nu/u_\tau$) and found that near the resonator's natural frequency, streamwise velocity fluctuation energy is amplified downstream, accompanied by a reduction in larger-scale energy. Hassanein *et al.* (2024) further investigated the scale-dependent coupling between the resonator's dynamics and the broadband turbulent velocity fluctuations, and introduced a conceptual model that aids in explaining the observed turbulence manipulation patterns. The conceptual model introduced by Hassanein *et al.* (2024) identifies three different frequency regimes of interaction with the Turbulent Boundary Layer (TBL): sub-resonance, resonance, and super-resonance, based on the impedance of HRs. When the resonator is excited by the wall-pressure fluctuations p'_{tbl} at sub-resonance, the induced velocity fluctuations v'_{o} at the orifice's exit plane (the wall) are in phase opposition to the incoming velocity fluctuations v'_{tbl}, leading to an attenuation of wall-normal and streamwise velocity fluctuations downstream. At resonance, the induced velocity fluctuations have relatively high magnitude and are in phase quadrature with the incoming velocity fluctuations. Consequently, downstream of the resonator, the velocity fluctuations are amplified and shifted in phase. At super-resonance, the induced velocity fluctuations are in phase alignment with the incoming velocity fluctuations. However, their magnitude is small, resulting in a negligible change in the energy of u and v fluctuations.

The work of Hassanein *et al.* (2024) and Dacome *et al.* (2024) shows that conventional miniature Helmholtz resonators inherently exhibit a bifurcated response: velocity fluctuations at sub-resonance frequencies are attenuated, whereas

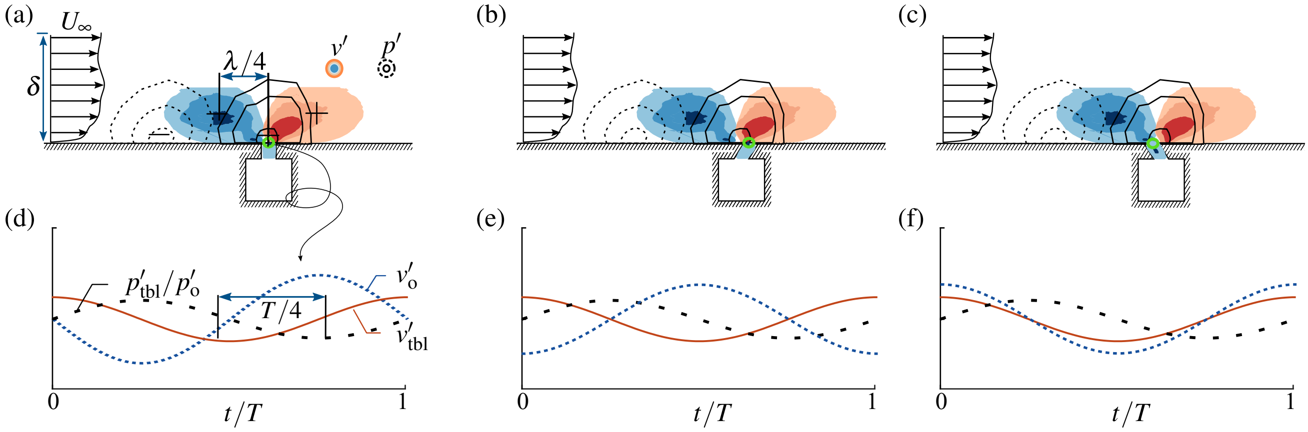

Figure 1: (a) A sketch of the conceptual model illustrating the interaction between a TBL and conventional Helmholtz resonator, as proposed by Hassanein *et al.* (2024), at the natural frequency of the resonator. (b–c) Conceptual schematics, based on this model, illustrating the phase change that occurs when the orifice is inclined at resonance: (b) the case where the orifice is aligned with the flow direction (positive inclination), and (c) the case where the orifice is aligned against the flow direction (negative inclination). (d–f) Time series of the pressure and velocity fluctuations plotted at the locations indicated by the green points in (a–c).

those at or above the resonance frequency are amplified. The concurrent manifestation of amplification and attenuation renders it difficult to exploit either effect exclusively. We hypothesise that inclining the orifice will lead to a spatial offset between the induced wall-normal velocity at the exit plane of the resonator and the wall-pressure fluctuations. Fig. 1 illustrates how this spatial offset can be realised, starting with Fig. 1(a), which shows the interaction between a conventional HR and wall-bounded turbulence at the resonance frequency, highlighting the phase quadrature between incoming velocity fluctuations and the induced wall-normal velocity fluctuations. The temporal phase difference at the resonator orifice is shown in Fig. 1(d). Note that the induced $v'_{\rm o}$ motion (negative in the sketch of Fig. 1(a); colored blue in the orifice) interacts in the green zone with the boundary layer-motion $v'_{\rm tbl}$ to yield a resultant, amplified energy within the grazing TBL flow. Figs. 1(b,c) illustrate our running hypothesis of how orienting the orifice to align with the direction of the flow (Fig. 1b) shifts the induced velocity to oppose the incoming fluctuations, whereas orienting it counter to the flow (Fig. 1c) shifts the induced wall-normal velocity to align with them.

LAYOUT OF EXPERIMENTS

Flow facility and Helmholtz resonator

Flow measurements were conducted in the Delft University Boundary Layer Facility (DU-BLF), integrated into the Small Low-Turbulence tunnel (SLT). In the present setup, the tunnel was operated in an open-loop configuration, with a TBL generated at the inlet of the test section. The TBL developed over a flat plate with a spanwise width of 0.90 m and a total streamwise length of 7.20 m under zero-pressure-gradient conditions. P40-grain sandpaper was applied along all sides at the start of the leading edge to force transition. Further details of the facility are provided by Knoop *et al.* (2026). In this work, a Cartesian coordinate system is defined at the centre of the HR orifice, located 6.10 m downstream of the leading edge and at the spanwise centre of the test section for the resonator cases. The flow conditions and TBL parameters of the nominal boundary layer at 6.10 m from the leading edge are summarised in Table 2. Here, $U_\tau = \sqrt{\tau_w/\rho}$ is the friction velocity, $l_\nu = \nu/U_\tau$ is the viscous length scale, and $Re_\tau = \delta/l_\nu$ is the friction Reynolds.

Measurements were carried out for six test cases: a baseline case without a resonator, and five cases with miniature HRs with orifices embedded at different angles. The acronyms for the resonator cases took the form HR-"P/N"θ. Here, "P/N" indicates the sign of the inclination angle, whether positive or negative, as defined in Fig. 2, and θ denotes the magnitude of the inclination angle. The resonator dimensions and the colour used for each case in the results section are shown in Table 1. Across all cases, the ratio of the natural frequencies of the resonators to the peak wall-pressure frequency, f_p^+, ranges from 0.98–1.09, where $f_p^+ \approx 0.04$ (Knoop *et al.*, 2026; Dacome *et al.*, 2025). It should be noted that l/d differs across cases, which influences the magnitude of the resonator-induced velocity. However, the data presented here are drawn from a larger dataset, and those variations are found to have a negligible effect on the principal conclusion of this study.

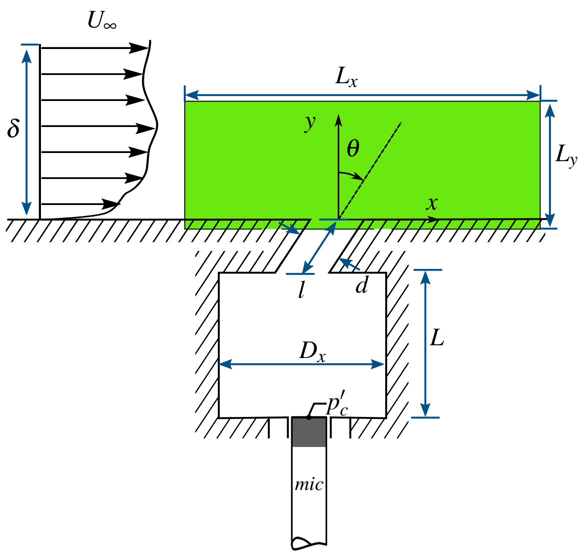

Figure 2: An illustrative schematic showing the HR, along with the relative position of the TR-PIV measurement, as well as the locations of the fluctuating pressure measurements p'_c.

Acronym	d (mm)	l (mm)	D_x (mm)	D_z (mm)	L (mm)	f_0 (Hz)	θ (°)	colour
HR-N70	4.35	5.80	24.31	36.46	52.01	350	-70	
HR-P70	4.35	5.80	24.31	36.46	52.01	350	70	
HR-N30	5.20	11.68	8.71	34.85	93.61	315	-30	
HR-P30	5.20	11.68	8.71	34.85	93.61	321	30	
HR-00	5.20	10.00	8.71	34.85	93.61	328	00	

Table 1: Properties of the Helmholtz resonator.

U_∞ (m/s)	Re_τ	δ (mm)	l_ν (μm)	U_τ (m/s)
9.6	2500	109	43.6	0.35

Table 2: Nominal TBL parameters.

Flow measurement systems

Time-resolved measurements of the cavity pressure fluctuations of the resonators, p'_c, were performed using GRAS 46BE 1/4-in pressure microphones. Location of the microphone capturing this signal is indicated in Fig. 2. The microphone sets possess a nominal sensitivity of 3.6 mV/Pa and maintain an accurate frequency response within ±1 decibel (dB, with a reference pressure of 20 μPa) in the range from 10 Hz to 40 kHz. The dynamic range spans from 35 to 160 dB.

Spatio-temporal velocity fields were obtained using double-framed two-dimensional, two-component time-resolved particle image velocimetry (2D2C TR-PIV). Water-glycol droplets of 1 μm diameter were used as flow tracers and were produced with a SAFEX smoke generator. Illumination was provided with a Quantronix Darwin-Duo 527 Nd:YLF laser (2x25 mJ @ 1 kHz). The thickness of the laser sheet was kept to 1 mm. Imaging was conducted using a FASTCAM Mini R5-4K camera ($4096 \times 2304\,\text{px}^2$ at 1250 fps, and a 6.5 μm pixel size). The active sensor area of each camera was cropped to $4096 \times 704\,\text{px}^2$, to accommodate the acquisition frequency that was set to 1.8 kHz. The resulting time separation between each image pair was $\Delta t = 45\,\mu$s, or in viscous units $\Delta t^+ = 0.36$. The camera was mounted on the side of the tunnel, where the resulting fields-of-view of $72 \times 13\,\text{mm}^2$; in viscous units, the fields of view measured $L_x^+ \approx 1650$ in the streamwise direction and $L_y^+ \approx 298$ in the wall-normal direction (see Fig. 2). A Nikon lens with a 200 mm focal length and an aperture $f_\#$ of 4 was used. The resulting image resolution was 64.4 px/mm (1 px = 15.53 μm = 0.36 l_ν). The PIV datasets comprised a total of 39 668 images pairs, divided into 4 ensembles of 9 917 uninterrupted image sequences. Note that the acquisition setup (i.e., the camera and the laser) remained the same across all test cases, and the test cases were changed via insert plates (refer to Knoop *et al.* (2026) to see the modular plate setup within the test section).

System synchronisation, image acquisition, and PIV processing were performed with the aid of LaVision's Davis 10.2 software. The processing of the time-resolved recordings is performed with the cross-correlations technique. The cross-correlation uses the multi-grid window deformation method, with a window size of $48 \times 12\,\text{px}^2$ for the final interrogation step and 75% overlap. Velocity vectors are obtained with a spacing of 6 px between adjacent points, corresponding to $\Delta y^+ \approx 2$. Finally, for each PIV dataset, the laser's Q-switch signal was acquired synchronously with the fluctuating pressure signals from the microphones in the resonator cavities. Sampling was performed using a NI 9234 DAQ module at a rate of 51.2 kHz and with a total of four ensembles, each lasting $T = 30$ s.

RESULTS

Spectral energy response of the TBL

To understand the effects of orifice inclination on velocity fluctuations, we begin by examining the spectrogram of the streamwise velocity fluctuations downstream of the orifice. The baseline case is shown in Fig. 3a, while Figs. 3(b,c,d) show the absolute difference in the streamwise velocity spectrogram between the resonator cases (HR-00, HR-N70, and HR-P70) and the baseline at $x^+ = 250$.

In the baseline spectrogram, the inner peak is well captured by the TR-PIV at $(y^+, f^+) \approx (15, 0.01)$. Across all resonator cases, a consistent trend can be observed: streamwise velocity fluctuations are amplified near the resonance frequency (indicated by the red-dashed line), while fluctuations at much lower frequencies are attenuated, consistent with the trend observed by Dacome *et al.* (2024); Hassanein *et al.* (2024). Furthermore, the inclination of the resonator orifice plays a significant role in manipulating streamwise velocity fluctuations within the TBL. Specifically, near resonance, HR-N70 exhibits the highest amplification amplitude and amplifies a broader band of frequencies compared to HR-00, where the orifice is not inclined. In contrast, HR-P70 shows a lower amplification amplitude and a reduced wall-normal extent compared to HR-00. The bands at which the velocity fluctuations are attenuated, are affected by orifice inclination as well. HR-N70 exhibits a higher attenuation magnitude than HR-00, albeit over a slightly narrower frequency band. HR-P70, on the other hand, shows both a wider attenuation band and a higher magnitude compared to the non-inclined resonator.

To further inspect how the orifice inclination affects the pattern of streamwise velocity fluctuations, we divide the velocity fluctuations into two frequency bands: low frequencies $f_{lf} = [0.008 : 0.015]$ and high frequencies $f_{hf} = [0.015 : 0.15]$ (indicated in Fig. 3). We then examine changes in the velocity-fluctuation energy of these two frequency bands in the spatial surroundings of the resonators. Fig. 4 shows the absolute difference in the premultiplied energy of the streamwise velocity fluctuations between the resonator cases and the baseline. Starting with the lower frequency band, shown in Figs. 4(a,c,e), the HR-N70 case shows amplification of velocity fluctuations around the orifice in a plume-like fashion, which decays by $x^+ = 200$, beyond which the velocity fluctuations are attenuated downstream until the edge of the measurement domain. Both HR-00 and HR-P70 show little to no amplification above the orifice, followed by an attenuation region. The HR-P70 case appears to have a more prominent attenuation region that extends beyond the measurement domain, compared to HR-00, where attenuation of the velocity fluctuations persists until approximately $x^+ = 600$. At the higher frequency band, shown in Fig. 4(b,d,f), the HR-N70 case amplifies velocity fluctuations significantly, reaching up

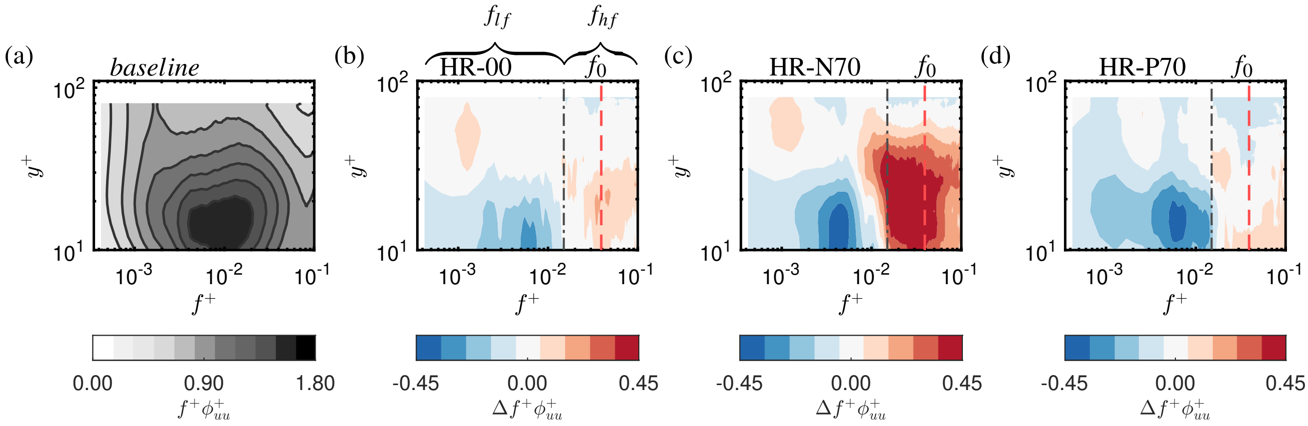

Figure 3: (a) Premultiplied energy spectrogram of the streamwise velocity fluctuations, $f^+\phi^+_{uu}$, for the baseline case. (b–d) Absolute differences with respect to the baseline, $\Delta f^+\phi^+_{uu}$, at $x^+ = 250$ for (b) the HR-00 case, (c) the HR-N70 case, and (d) the HR-P70 case.

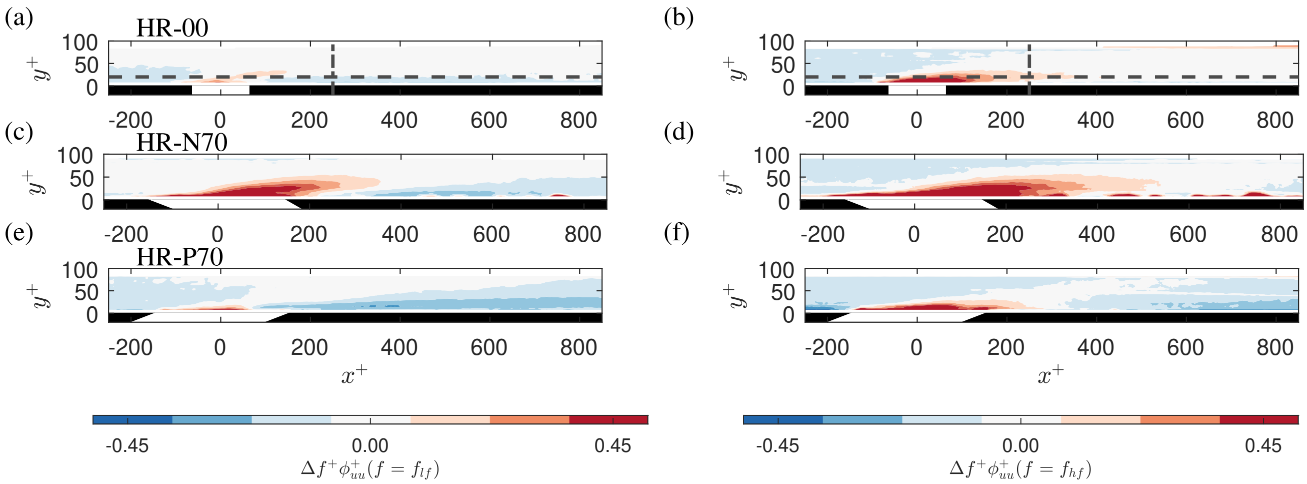

Figure 4: (a–f) Contours of the absolute differences, relative to the baseline, of the premultiplied energy of the streamwise velocity fluctuations, $\Delta f^+\phi^+_{uu}$. (a,c,e) correspond to the low-frequency band f_{lf} for the HR-00, HR-N70, and HR-P70 cases, respectively, and (b,d,f) correspond to the high-frequency band f_{hf}. The horizontal dashed lines indicate the locations of the plots shown in Fig. 5 and the vertical dashed lines indicate the position of the spectrograms shown in Fig. 3.

to $0.9U_\tau^2$, with the amplification region extending up to $50l_\nu$ in the wall-normal direction and up to $x^+ = 500$ in the streamwise direction. In contrast, HR-P70 shows a small region of amplification limited to the orifice extent in the streamwise direction and $15l_\nu$ in the wall-normal direction, followed by an attenuation of the streamwise velocity fluctuations downstream of the orifice.

To understand whether this trend holds for smaller angles, we examine the absolute difference in the premultiplied energy of the streamwise velocity fluctuations between the resonator cases and the baseline at $y^+ = 15$ for all resonator cases, shown in Fig. 5. At low frequencies, the velocity fluctuations around the orifice show a trend of amplification that appears to decay with increasing orifice inclination, with almost no amplification for the HR-P70 case. Downstream of the orifice, no clear trend in the attenuation magnitude is observed. It is worth noting that the two extreme inclination cases, HR-P70 and HR-N70, exhibit the highest attenuation magnitude downstream of the orifice. At higher frequencies, the amplification of the velocity fluctuations follows a clear trend: the amplification amplitude decreases monotonically as the orifice inclination angle varies from negative to positive, with the HR-P70 case showing attenuation of velocity fluctuations downstream of the orifice. The trend observed in the spectral energy of the velocity fluctuations supports the initial hypothesis of this work: the inclination of the orifice provides additional control authority over near-wall velocity fluctuations. By inclining the orifice in the positive direction, the prominence of resonance in amplifying velocity fluctuations is reduced, and a broader frequency band of attenuation is achieved. Conversely, inclining the orifice in the negative direction leads to a more prominent amplification of velocity fluctuations over a broader frequency band.

Resonator-turbulence interaction

This section is aimed at understanding whether the inclination of the orifice skews the phase between the velocity fluctuations and the wall-pressure fluctuations exciting the resonator, which in turn drives the observed pattern of turbulent velocity fluctuation manipulation. To this end, we begin by examining the coherence between the pressure fluc-

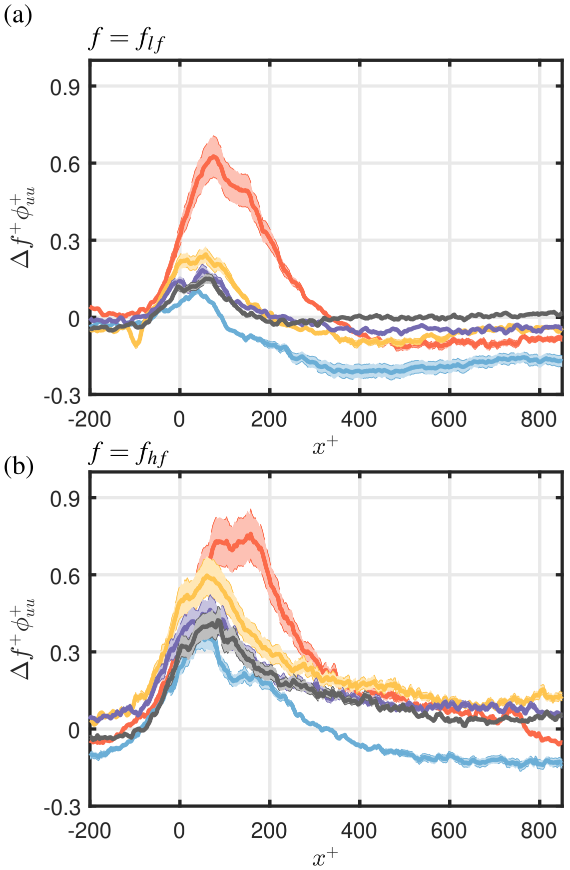

Figure 5: Plots of the absolute differences, relative to the baseline, of the premultiplied energy of the streamwise velocity fluctuations, $\Delta f^+\phi^+_{uu}$ at $y^+ = 15$. (a) Correspond to $f = f_{lf}$, and (b) correspond to $f = f_{hf}$.

tuations inside the cavity and the velocity fluctuations, with the goal of inferring the degree to which the resonator dynamics are coupled. The cavity pressure is selected over the wall-pressure fluctuations because it correlates highly with the latter, whereas the wall-pressure fluctuations cannot be measured directly in the current setup. To investigate the connection between the fluctuations of wall-pressure and wall-normal velocity, we evaluate the coherence between the cavity pressure and the wall-normal velocity above the resonator exit plane, as shown in Fig. 6(a). This provides insight into the extent to which the wall-pressure fluctuations — viewed as the energy source for the resonator system and the response of the resonator (Hassanein *et al.*, 2024) — are correlated across frequencies, and thus the range over which the wall-normal velocity is dominated by the induced velocity of the resonator or the existing wall-normal velocity fluctuations in the TBL.

The coherence, $\gamma^2_{p_c v_r}(f)$, is defined in equation 1, where the subscripts p_c is the cavity pressure and v_r is wall-normal velocity box-averaged over the range $x^+ \in [-0.5d, 0.5d]$, $y^+ \in [0, 0.3d]$. The one-sided cross-spectrum of the quantity p_c is given by $\phi_{p_c v_r}(f) = 2\langle \widehat{p}_c(f)\,\widehat{v}^*_r(f)\rangle$, and the auto-spectra, $\phi_{p_c p_c}(f)$ and $\phi_{v_r v_r}(f)$, are defined analogously.

$$\gamma^2_{p_c v_r}(f) = \frac{\left|\phi_{p_c v_r}(f)\right|^2}{\phi_{p_c p_c}(f)\,\phi_{v_r v_r}(f)}\,. \qquad (1)$$

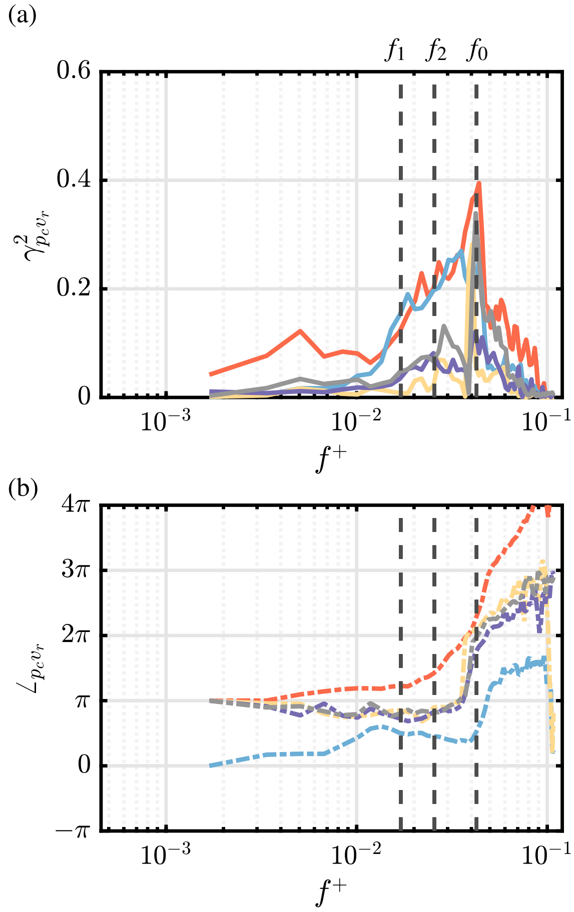

Figure 6: (a) Coherence between the cavity pressure p_c and the wall-normal velocity fluctuations above the orifice v_r. (b) phase difference between the cavity pressure p_c and the wall-normal velocity fluctuations above the orifice v_r.

Figure 6(a) presents the coherence between the cavity pressure and the resultant wall-normal velocity above the orifice of the resonators. In all cases, the coherence near resonance is high, indicating that the wall-normal velocity is dominated by the resonator-induced velocity at these frequencies. Furthermore, the highly inclined cases, HR-P70 and HR-N70, exhibit higher coherence at sub-resonant frequencies. At very low frequencies (below $f^+ = 0.005$), the incoming turbulent fluctuations appear to dominate the wall-normal velocity above the orifice, causing the coherence between the cavity pressure and the wall-normal velocity to drop to near-zero values.

We now consider the phase between the cavity pressure p_c and the wall-normal velocity v_r, denoted $\angle_{p_c v_r}$. Figure 6(b) shows the phase difference between the cavity pressure and the wall-normal velocity for all resonator configurations. A clear monotonic trend is observed: $\angle_{p_c v_r}$ decreases steadily as the orifice inclination angle varies from the most negative to the most positive. This behaviour is consistent across all frequencies, although the magnitude of the variation differs. More noteworthy, significant differences in $\angle_{p_c v_r}$ are observed between the non-inclined orifice HR-00 and the inclined configurations. For brevity, we focus on the most extreme cases, HR-N70 and HR-P70, where the deviation in $\angle_{p_c v_r}$ relative to HR-00 increases with frequency. This behaviour can be interpreted in terms of the diameter-to-wavelength ratio DWR,

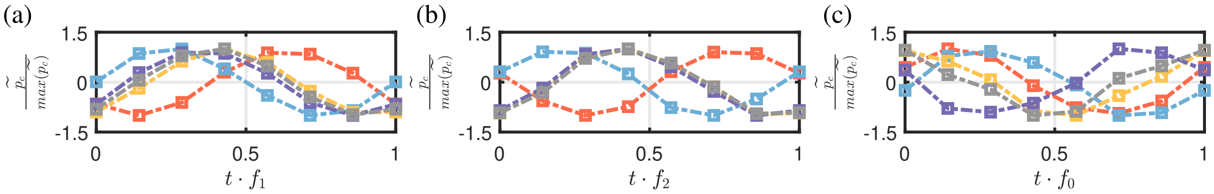

Figure 7: (a) Normalised conditionally averaged cavity pressures p_c, using the wall-normal velocity above the orifice v_r at (a-b) two sub resonant frequencies $f_1 = 0.6 \times f_0$, $f_2 = 0.8 \times f_0$, respctively, and (c) the natural frequency $f_0^+ = 0.04$.

defined as the ratio of the apparent diameter $\widetilde{d}^+ = d^+/\cos(\theta)$ to the wavelength of the velocity fluctuations $\lambda^+ = U_c^+/f^+$. The diameter-to-wavelength ratio is therefore given by:

$$DWR = \frac{\widetilde{d}^+}{\lambda^+} = \frac{d^+/\cos(\theta)}{U_c^+/f^+}, \tag{2}$$

where U_c^+ is the convection velocity, taken here as $U_c^+ = 10$. A larger diameter-to-wavelength ratio indicates that the orifice inclination skews the phase relationship between the wall-pressure fluctuations and the wall-normal velocity fluctuations more strongly, which is subsequently reflected in the phase difference between the cavity pressure and the wall-normal velocity fluctuations. This effect becomes more pronounced at higher frequencies, where the shorter wavelengths increase the relative importance of the apparent diameter, leading to a greater phase shift within a single oscillation period. This reasoning also explains why the moderately inclined cases, HR-P30 and HR-N30, exhibit noticeable phase differences relative to the non-inclined case only at higher frequencies.

To further understand the effect of inclining the orifice on the phase relationship between the wall-pressure fluctuations and the wall-normal velocity fluctuations, we examine the cavity pressure fluctuations conditioned on the wall-normal velocity fluctuations above the orifice at three selected frequencies: two sub-resonance frequencies, $f_1 = 0.6 \times f_0$ and $f_2 = 0.8 \times f_0$, and the resonance frequency f_0, indicated in Fig. 6. The natural frequency is taken as $f^+ = 0.04$ here. When inspecting the normalised conditionally averaged pressure fluctuations $\widetilde{p_c}$ at f_1, shown in Fig. 7(a), $\widetilde{p_c}$ of the non-inclined orifice HR-00 leads that of the negatively inclined orifices, with the HR-N70 case exhibiting the largest lag of a quarter of a period. The positively inclined orifice shows a mirrored response, with $\widetilde{p_c}$ of HR-P70 leading that of HR-00 by the same amount. The moderately inclined cases appear to follow this trend, but with a very small phase shift. At the higher sub-resonance frequency f_2, shown in Fig. 7(b), a similar trend is observed, but the inclination now causes the signals to drift by almost half a period. At resonance, shown in Fig. 7(c), the signals of the most inclined cases, HR-P70 and HR-N70, have drifted to the point where both share the same relative phase. In the moderately inclined cases, a noticeable phase difference begins to appear at this frequency. These observations explain why the HR-N70 case amplifies a wider range of frequencies: the range of frequencies over which the induced velocity fluctuations from the resonator are in phase with the incoming velocity fluctuations is wider. For the HR-P70 case, on the other hand, this range is narrower, and at resonance, the phase drift is more pronounced because the DWR is higher (DWR ≈ 1.12), leading to the amplification of velocity fluctuations being concentrated near resonance.

CONCLUSIONS

This work explored a new means of controlling near-wall turbulence by inclining the orifice of a miniature Helmholtz resonator. The work began with the hypothesis that inclining the orifice would lead to a shift in the phase between the induced velocity fluctuations of the resonator and the wall-pressure fluctuations exciting it. TR-PIV was used for flow measurements, focusing on five inclination angles ranging from $\theta = -70°$ to $\theta = 70°$, where positive angles point in the streamwise direction. Our results reveal that inclining the orifice manipulates the turbulence in the manner hypothesised. The most negatively inclined case exhibits a broader range of frequencies over which the velocity fluctuations are amplified compared to the non-inclined orifice. On the other hand, the most positively inclined case attenuates velocity fluctuations over a broader range of frequencies and amplifies a narrower band of velocity fluctuations, suggesting that orifice inclination can skew the phase between the induced wall-normal velocity and the wall-pressure fluctuations exciting the resonator. This phase skewing was further investigated by examining the phase between the cavity pressure and the wall-normal velocity fluctuations above the orifice, confirming that the inclination induces a drift in phase. Further investigation reveals that this skewing is dependent on the ratio of the apparent diameter to the wavelength of the velocity fluctuations, termed here the diameter-to-wavelength ratio, where the velocity fluctuations drift further from the pressure fluctuations at higher DWR. This identifies the DWR as an important parameter to consider when designing a resonator for controlling near-wall turbulence. The results of this work open new avenues for the use of Helmholtz resonators to predeterministically attenuate or amplify wall-bounded turbulence across targeted frequency bands.

REFERENCES

Dacome, G., Lazzarini, L., Talamelli, A., Bellani, G. & Baars, W. J. 2025 Scaling of wall-pressure–velocity correlations in high-Reynolds-number turbulent pipe flow. *J. Fluid Mech.* **1013**, A48.

Dacome, G., Siebols, R. & Baars, W. J. 2024 Small-scale Helmholtz resonators with grazing turbulent boundary layer flow. *J. Turbul.* **25** (12), 461–481.

Flynn, K. P., Panton, R. L. & Bogard, D. G. 1990 Effect of Helmholtz resonators on boundary-layer turbulence. *AIAA J.* **28** (11), 1857–1858.

Hassanein, A., Modesti, D., Scarano, F. & Baars, W. J. 2024 Interaction of an inner-scaled Helmholtz resonator with boundary-layer turbulence. *Phys. Rev. Fluids* **9** (11), 114610.

Knoop, M. W., Hassanein, A. & Baars, W. J. 2026 Development and characterisation of a turbulent boundary layer facility at the Delft University of Technology. *Aerospace Sci. Technol.* **168**, 110972.